CIRP Annals - Manufacturing Technology 67 (2018) 169–172

Contents lists available at ScienceDirect

CIRP Annals - Manufacturing Technology

journal homepage: http://ees.elsevier.com/cirp/default.asp

Digital twin driven prognostics and health management for complex equipment

Fei Tao [a], Meng Zhang [a], Yushan Liu [a], A.Y.C. Nee (1)[b,*]

[a] School of Automation Science and Electrical Engineering, Beihang University, Beijing 100191, PR China
[b] Department of Mechanical Engineering, National University of Singapore, Singapore 117576, Singapore

ARTICLE INFO

Article history:
Available online 24 May 2018

Keywords:
Maintenance
Condition monitoring
Digital twin

ABSTRACT

Prognostics and health management (PHM) is crucial in the lifecycle monitoring of a product, especially for complex equipment working in a harsh environment. In order to improve the accuracy and efficiency of PHM, digital twin (DT), an emerging technology to achieve physical–virtual convergence, is proposed for complex equipment. A general DT for complex equipment is first constructed, then a new method using DT driven PHM is proposed, making effective use of the interaction mechanism and fused data of DT. A case study of a wind turbine is used to illustrate the effectiveness of the proposed method.

1. Introduction

Complex equipment such as aircrafts, ships, wind turbines are designed to work over decades in harsh environment. Thus, performance degradation is inevitable during its operation, which can lead to malfunctioning, resulting in high maintenance costs. Prognostics and health management (PHM) has been introduced for the reliable operation of complex equipment. It is used to monitor the equipment condition, perform the diagnosis and prognosis, and provide design rules for maintenance [1].

However, most current works on PHM are primarily driven by the equipment in its physical space, with little connection to its virtual model. Currently, with the development of cyber-physical system (CPS), it is critical to attach importance to the virtual space and implement the seamless convergence of physical and virtual spaces, to improve the PHM for complex equipment. In this context, in the virtual space, a digital mirror of the equipment and its data are introduced to depict the behaviour of the real entity. Some potential applications have been explored in Ref. [2], however, to implement PHM driven by both physical and virtual spaces, some outstanding common issues still exist. They include (1) building the high-fidelity digital mirror to describe the equipment thoroughly; (2) establishing the interaction between the equipment and its digital mirror to make them support PHM seamlessly; (3) converging the data from physical space and virtual space to generate accurate information for PHM.

In this paper, digital twin (DT), a reference model for the physical–virtual convergence, is applied to address the above three issues. *Firstly*, based on DT, a high-fidelity digital mirror model for the equipment is built in different levels of geometry, physics, behaviour and rule. It provides access to the equipment even out of physical proximity. *Secondly*, the interaction mechanism of DT can detect the disturbances from the environment, potential faults in the equipment and defects in the models. It is a coupled optimization to make the equipment and digital model evolve continuously. *Thirdly*, since DT includes data from the equipment, the digital model, and the fused data, data for PHM can be enriched greatly to provide accurate information.

In this study, a five-dimension DT for complex equipment is first established, then a new approach for PHM driven by DT for complex equipment is proposed, and its framework and workflow are explored in detail. A case study of a wind turbine is presented to show the effectiveness of the proposed new method.

2. Five-dimension DT model

A general and standard architecture for DT model was first built by Grieves [3]. In this architecture, the DT is modelled in three dimensions, i.e. the physical entity, virtual model and connection, and is characterized by the physical–virtual interaction. It has been applied to product design and production [4,5]. Based on this, an extended five-dimension architecture DT is proposed in this paper, adding DT data and services. Compared with Grieves' architecture, besides the physical–virtual interaction, the proposed model fuses data from both the physical and virtual aspects using DT data for more comprehensive and accurate information capture. It can also encapsulate the functions of DT (e.g. detection, judgement and prediction) from the services for unified management and on-demand usage [6].

According to the proposed five-dimension architecture, Fig. 1 shows the proposed DT for complex equipment, which can be depicted as in the following expression,

$$M_{DT} = (PE, VE, Ss, DD, CN) \quad (1)$$

* Corresponding author.
E-mail address: mpeneeyc@nus.edu.sg (A.Y.C. Nee).

https://doi.org/10.1016/j.cirp.2018.04.055
0007-8506/

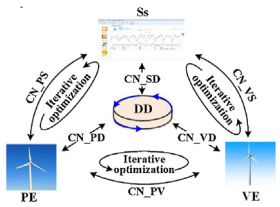

Fig. 1. Five-dimension DT model for complex equipment.

where *PE* refers to the physical entity, *VE* is the virtual equipment, *Ss* stands for services for *PE* and *VE*, *DD* refers to DT data, and *CN* is the connection among *PE*, *VE*, *Ss* and *DD*. To illustrate the proposed DT for complex equipment, a wind turbine (WT) is considered in a case study.

2.1. Physical entity model (PE)

Generally, *PE* consists of the various functional subsystems and sensory devices. Subsystems perform the predefined tasks during operation and sensors collect the states of the subsystems and working conditions. Malfunctioning of any part may cause the *PE* to fail. In Fig. 2, the functional subsystems of a WT consist of the blade, generator, gearbox, yaw system, etc. for transforming wind energy into mechanical and electrical energy. Sensors are deployed to collect the generator temperature, gearbox vibration, power output, etc.

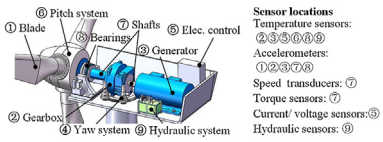

Fig. 2. Physical WT model.

2.2. Virtual equipment model (VE)

VE is a high fidelity digital model of the *PE*, which integrates multiple variables, scales and abilities of the *PE* to reproduce its geometries, physical properties, behaviours and rules in the virtual world. *VE* is modelled as follows,

$$VE = (Gv, Pv, Bv, Rv) \quad (2)$$

where G_v, P_v, B_v and R_v, stand for the geometry model, physics model, behaviour model and rule model, respectively. The modelling of *VE* is interpreted as follows, combining with the construction of the virtual WT model in Fig. 3.

G_v is constructed as a 3D solid model. The WT components (e.g. gearbox, blade and shaft) are assembled using a commercial CAD modelling software.

P_v simulates the physical properties of the *PE*. For the WT, blade deformation, gear tooth stress and bearing temperature, etc. can be simulated in this level using the finite element method (FEM).

B_v describes the behaviour of the *PE* governed by the driving factors (e.g. control orders) or disturbing factors (e.g. human interferences). Behaviour of the WT includes power generation, yawing, pitching, untwisting, etc. Power generation is a function of the wind speed and power transmission efficiency, while yawing is expressed as the relation among the yaw angel (φ_y), yaw rate (ω_y), and yaw error (*err*) [7].

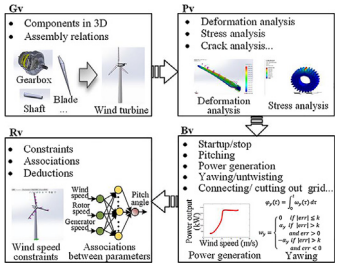

Fig. 3. Virtual WT model.

R_v includes rules of constraints, associations and deductions. The rules work as the 'brain' to make the *VE* judge, evaluate, optimize and/or predict. For the WT, constraints for the wind speed can be simulated through force analysis and associations of parameters can be mined from cloud data using neural network.

By the constructed *VE*, G_v, P_v, B_v and R_v are coupled in functions and structures to form a complete mirror image of the *PE*.

2.3. Services model (Ss)

Ss includes services for *PE* and *VE*. It optimizes the operations of the *PE*, and ensures the high fidelity of the *VE* through calibrating the *VE* parameters during its running to sustain its performance with the *PE*. *Ss* consists of elements as in (3), which describes the function, input, output, quality and state of services. *Ss* can be scheduled to meet the demands of the *PE* and *VE*.

$$Ss = (Function, Input, Output, Quality, State) \quad (3)$$

Take the power output monitoring service for the physical WT model as an example. It can be represented as Ss_monitor = (Power output monitoring, (wind speed, power output of physical WT, power output of virtual WT), power condition, (time, cost, reliability), (work, idle, failure)).

2.4. DT data model (DD)

DD includes five parts as denoted in (4),

$$DD = (Dp, Dv, Ds, Dk, Df) \quad (4)$$

where D_p is the data from the *PE*, D_v is the data from the *VE*, D_s is the data from the *Ss*, D_k represents the domain knowledge, and D_f denotes the fused data of D_p, D_v, D_s and D_k. *DD* includes data from both physical and virtual aspects as well as their fusion, which enriches the data greatly. Fig. 4 shows the *DD* of the WT.

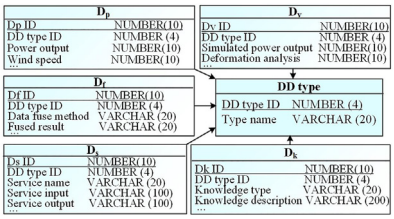

Fig. 4. *DD* of the WT.

2.5. Connection model (CN)

CN includes six parts as expressed in (5),

$$CN = (CN\_SD, CN\_PD, CN\_VD, CN\_PS, CN\_VS, CN\_PV) \quad (5)$$

where *CN_SD*, *CN_PD*, *CN_VD*, *CN_PS*, *CN_VS*, and *CN_PV* denote the connection between *Ss* and *DD*, *PE* and *DD*, *VE* and *DD*, *PE* and *Ss*, *VE* and Ss, *PE* and *VE*, respectively. Each connection (denoted as *CN_XX*) is bidirectional and the delivered data is modelled in (6).

$$CN_XX = (Datasource, Unit, Value, Scope, Sampling\ interval) \quad (6)$$

Take *CN_PV* for the WT as an example. Data from the physical WT (e.g. yaw angle) is expressed as CN_PV_yaw_angle = (Physical WT, degree, 10, 0-1080, 10s). Order from the virtual WT (e.g. yaw rate) is denoted as CN_PV_yaw_order = (Virtual WT, rad/s, 8.7e-3, 0-(1.7e-2), 10s).

3. DT driven PHM method

The established DT is then applied to create the DT driven PHM method shown in Fig. 5. In this method, faults are classified into gradual fault and abrupt fault. The former can be predicted as caused by the gradual component degradation. The latter is unpredictable and happens suddenly due to disturbances.

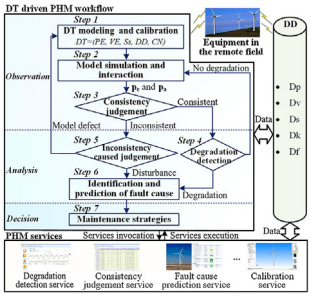

Fig. 5. Framework and workflow of DT driven PHM method.

There are three stages in the workflow in Fig. 5, i.e. *observation (steps 1 – 3)*, *analysis (steps 4 – 6)* and *decision (step 7)*.

Step 1: DT modelling and calibration. Establish the DT for the complex equipment according to Section 2. If the *VE* deviates from the *PE*, there are two possible ways to eliminate the deviation: (1) calibrate the *VE* through parameters tuning based on the least-squares method [8]; (2) maintain *CN_PV* to ensure the real-time communication between the *PE* and *VE*.

Step 2: Model simulation and interaction. Let $X=\{x_i|0 \le i \le n\}$ and $C=\{c_j|0 \le j \le m\}$ denote the real-time states and working conditions collected from the *PE*, where x_i is the ith actual state (e.g. speed, torque, force), c_j is the jth condition (e.g. environment, load, control order), while n and m are the element number. Load X and C to *VE* for initialization and simulation, and denote the outputs of VE as $Y=\{y_i| 0 \le i \le n\}$ and $Z=\{z_k|0 \le k \le l\}$, where y_i is the mapping to x_i, expressing the ith simulated state, z_k denotes other analysis result (e.g. stress analysis), while n and l are the element number. *PE* and *VE* are kept interactive to ensure both can reach the latest states.

Step 3: Consistency judgement. Select t elements from X and Y ($t \le n$). Then let $\boldsymbol{p_a}=(x_1 \dots x_i \dots x_t)$ and $\boldsymbol{p_e}=(y_1 \dots y_i \dots y_t)$ denote the states of *PE* and *VE* at the current moment (assumed as t_n) respectively, where $x_i \in X$ and $y_i \in Y$. If $\mathbf{p_e}-\mathbf{p_a} \le T_p$, where T_p is a predefined threshold, treat *PE* and *VE* as consistent, meaning within the tolerable differences caused by inevitable fluctuations (e.g. changes in the actual environment). Then go to Step 4. Otherwise, they are inconsistent and go to Step 5.

Step 4: Degradation detection. With the operation of *PE*, performance degradation will appear. It can be reflected on indicators expressed by the data from X, Y and Z. If some indicators exceed the thresholds, the *PE* has degraded and the gradual fault will occur with the accumulation of the degradation, then go to Step 6. Otherwise, go to Step 2.

Step 5: Inconsistency caused judgement. Take the time series of historical states of *PE* under the same condition (i.e. C) as the reference to decide if the inconsistency is caused by either *PE* or *VE*. Represent the reference as $\boldsymbol{P_{hs}}=(\boldsymbol{x_{hs1}} \dots \boldsymbol{x_{hsi}} \dots \boldsymbol{x_{hst}})$, where t is the element number, $\boldsymbol{x_{hsi}}$ is the time series for the ith parameter, denoted as $\boldsymbol{x_{hsi}}=x_{hsi}(1) \dots x_{hsi}(q) \dots x_{hsi}(s))^T$ and s is the element number. Accordingly, for the ith parameter in $\boldsymbol{p_a}$ (i.e. x_i) and $\boldsymbol{p_e}$(i.e. y_i), the time series from the current moment (i.e. t_n) to t_{n+s-1} are denoted as $\boldsymbol{x_{si}}=(x_{si}(1) \dots x_{si}(q) \dots x_{si}(s))^T$ and $\boldsymbol{y_{si}}=(y_{si}(1) \dots y_{si}(q) \dots y_{si}(s))^T$, respectively. Denote $\boldsymbol{P_{as}}=(\boldsymbol{x_{s1}} \dots \boldsymbol{x_{si}} \dots \boldsymbol{x_{st}})$ and $\boldsymbol{P_{es}}=(\boldsymbol{y_{s1}} \dots \boldsymbol{y_{si}} \dots \boldsymbol{y_{st}})$ as the time series for $\boldsymbol{p_a}$ and $\boldsymbol{p_e}$. Measure the similarity of $\boldsymbol{P_{as}}$ and $\boldsymbol{P_{hs}}$, as well as $\boldsymbol{P_{es}}$ and $\boldsymbol{P_{hs}}$ according to the correlation based dynamic time warping method [9]. If only $\boldsymbol{P_{es}}$ is similar with $\boldsymbol{P_{hs}}$, the inconsistency is caused by the abrupt fault of the *PE*, due to the sudden disturbance unknown to *VE*, then go to Step 6. If only $\boldsymbol{P_{as}}$ is similar with $\boldsymbol{P_{hs}}$, the inconsistency is caused by the model defect, then go to Step 1. If both $\boldsymbol{P_{as}}$ and $\boldsymbol{P_{es}}$ are dissimilar with $\boldsymbol{P_{hs}}$, go to Step 1 for model calibration first.

Step 6: Identification and prediction of fault cause. Two conditions are classified according to Steps 4 and 5 as follows:

(1) Gradual fault: From Step 4, before the complete failure, localize the fault cause. It includes two phases. In the training phase, extract forewarning features from historical data of X, Y and Z. Then train prediction models to fuse the features and relate them to fault causes by methods such as neural network. In the prediction phase, input features from the real-time data of X, Y and Z into the trained models and predict the fault cause.
(2) Abrupt fault: From Step 5, localize the components related to the abrupt fault first. Then check the components one by one through comparing parameters from the *VE* with those from the *PE*, to finally identify the source of disturbance as the fault cause.

Step 7: Maintenance strategies. According to the fault cause, select the maintenance strategies among a set of standby alternatives. Perform the selected strategies on the *VE* first for validation, then carry them out on the *PE*.

As per framework shown in Fig. 5, the functions needed in the method (e.g. consistency judgement, fault cause prediction, calibration) are realized by the corresponding services. Data from the workflow are stored in *DD*, and they are sent back after processing (e.g. data fusion) to drive these steps. Meanwhile, data from the remote equipment are also updated continuously.

In summary, the PHM process must consider both the physical and virtual aspects by fusing signals collected from the *PE* and those simulated by the *VE*. Accurate predictions are particularly important in PHM. With DT, predictions are mainly effected as follows. (1) The deviation of two parts in the PE and VE would reflect inconsistency and provides indications of potential failure occurrence. (2) As signals from both PE and VE can be obtained and fused completely, predictions can be performed more accurately.

4. Case study

4.1. Problem description

A WT is a complex equipment which transforms wind energy to electrical energy. Since a WT is designed to last decades and its working conditions are characterized by stochastic load, varying torque and dusty environment, most components may fail during operation [10]. However, it is not practical to access the WT all the time. The constructed DT for the WT in Section 2 is able to address this with the DT driven PHM method in Section 3.

The gearbox, as part ② in Fig. 2, is one of the most failure prone elements of a WT [11]. Its failure is mainly caused by the gradual degradation. This section considers the gearbox as the example to demonstrate the proposed method.

4.2. Verification of the proposed DT driven PHM method

According to Steps 1 and 2 in Section 3, with the constructed DT for the WT, the simulation and interaction are started. According to Step 3, the states of the gearboxes in the physical and virtual WTs are presented as $\boldsymbol{p_a}=(T_{ai}, T_{ao})$ and $\boldsymbol{p_e}=(T_{ei}, T_{eo})$, respectively. T_{ai} and T_{ao} are collected from the torque sensors installed on the input and output shafts (part ⑦ in Fig. 2), while T_{ei} and T_{eo} are simulated on the virtual WT based on the transmission relations among the wind wheel, gearbox and generator. The deviation of p_a and p_e is calculated according to Eq. (7) and T_p is set to 6% based on the experience. As $\mathbf{p_e}-\mathbf{p_a} \le T_p$ is satisfied, the gearboxes of the physical and virtual WTs are consistent.

$$\| \boldsymbol{p_e}-\boldsymbol{p_a} \| = \frac{\sqrt{(T_{ei}-T_{ai})^2+(T_{eo}-T_{ao})^2}}{\sqrt{(T_{ai})^2+(T_{ao})^2}} \tag{7}$$

Table 1
A list of symbols.

Symbols of gearbox in physical WT		Symbols of gearbox in virtual WT	
T_{ai}	Input torque	T_{ei}	Input torque
T_{ao}	Output torque	T_{eo}	Output torque
FC	Frequency centre	T_{cm}	Maximum contact stress
VF	Frequency variance	T_{rm}	Maximum bending stress
MSF	Mean square frequency	N_m	Number of gear meshing

According to Step 4, vibrations are collected by accelerometers mounted on the gearbox. The energy for every 1000 samples of the vibration time series is calculated as $\sum_{i=1}^{1000}|a_i|^2$, where a_i is the amplitude for the ith sample. If it exceeds the maximum value, the gearbox has degraded. Related symbols are listed in Table 1.

According to Step 6, the fault cause (i.e. *tooth wear, fatigue* or *breakage*) prediction process is shown in Fig. 6. From the gearbox in the physical WT, the vibration frequencies show different positions and energies for different fault causes, which can be reflected on *FC*, *VF* and *MSF* of the vibration frequency spectrums in Fig. 6(a). Hence, *FC*, *VF* and *MSF* are selected as forewarning features. Furthermore, from the gearbox in the virtual WT, since the different fault causes can be reflected on the different stress levels (e.g., contact stress and bending stress in Fig. 6(b)) on the tooth, T_{cm}, T_{rm} and N_m are selected as forewarning features. T_{cm} and T_{rm} can be got by analysing the forces acting on the tooth surface and root, and N_m can be obtained by recording the gear meshing number. Then the extreme learning machine (ELM) [12], a single-hidden layer network with fast learning speed and good generalization performance, constructs the fault cause prediction model as shown in Fig. 6(c), of which the inputs are *FC*, *VF*, *MSF*, T_{cm}, T_{rm} and N_m. Finally, based on the inputs and constructed model, in Fig. 6(d), the output identifies the fault cause.

According to Step 7, the maintenance strategy suggests welding repair. The welding process is first carried out to the gearbox in the virtual WT for validation, then performed on the gearbox in the physical WT. The proposed method does not access the WT, while predicting the fault cause and maintaining procedure.

4.3. Performance comparisons and analysis

The traditional fault cause prediction method for gearboxes usually uses vibration signals from the gearbox in the physical WT (denoted as *P-Method*). To further validate the advantages of the proposed DT driven method (denoted as *DT-Method*), its performance is compared with the *P-Method*. In this case, the *P-method* is also built using the ELM. The inputs of the *P-Method* are FC, *VF* and *MSF*, which are also used in the DT-Method. The two methods are tested on 40 WTs data with degraded gearboxes, 15 for tooth wear, 13 for tooth fatigue and 12 for tooth breakage.

For the three conditions (i.e. *tooth wear, fatigue and breakage)*, the number of WTs identified into the correct condition by each method are shown in Fig. 7. Compared with the *P-method*, the accuracy of *DT-Method* has improved clearly.

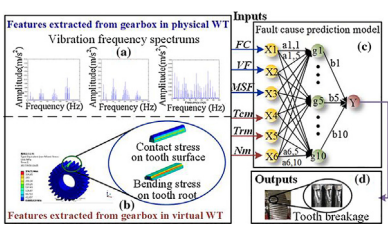

Fig. 6. Fault cause prediction of gearbox driven by DT.

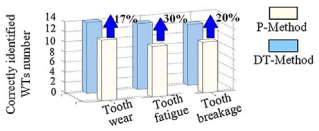

Fig. 7. Accuracy comparisons of two methods.

The advantage of the DT-method mainly comes from its construction. According to the workflow, under the premise that the gearboxes in the physical and virtual WTs are consistent, the constructed DT can fuse the vibration and stress signals for prognosis. It can depict the gearbox from both the physical and virtual aspects. However, the P-Method only focuses on the vibration signals from the physical WT. As the signals are prone to interferences from other vibration sources, the accuracy of the P-Method can be affected easily.

5. Conclusions and future work

In the paper, the DT driven PHM has been proposed for complex equipment. Using the WT as an illustration, the five-dimension DT is first proposed and established. Then the framework and workflow of the DT driven PHM are presented and a case study of gearbox prognosis is performed to confirmed the proposed *DT-method* for improving the accuracy of prognosis.

Considering the implementation costs and complexity of DT, the proposed DT driven PHM method will be useful for monitoring high-value and major equipment in a plant, and there must be sufficient data for DT modelling. To scale up the PHM application, challenges mainly include: (1) constructing high-fidelity digital mirrors for complex equipment with different properties and behaviours; (2) processing large amount of DT data; (3) balancing costs and benefits of the DT.

Acknowledgments

This work is supported in part by the NSFC project (No. 51522501). The authors thank DHC Software Co., Ltd for providing information and data in this research.

References

[1] Gao R, Wang LH, Teti R, Dornfeld D, Kumara S, Mori M, Helu M (2015) Cloud-enabled Prognosis for Manufacturing. *CIRP Annals — Manufacturing Technology* 64(2):749–772.
[2] Lee J, Bagheri B, Kao HA (2015) A Cyber-Physical Systems Architecture for Industry 4.0-based Manufacturing Systems. *Manufacturing Letters* 3:18–23.
[3] Grieves M (2014) *Digital Twin: Manufacturing Excellence through Virtual Factory Replication, White Paper.*
[4] Schleich B, Anwer N, Mathieu L, Wartzack S (2017) Shaping the Digital Twin for Design and Production Engineering. *CIRP Annals — Manufacturing Technology* 66(1):141–144.
[5] Söderberg R, Wärmefjord K, Carlson JS, Lindkvist L (2017) Toward a Digital Twin for Real-time Geometry Assurance in Individualized Production. *CIRP Annals — Manufacturing Technology* 66(1):137–140.
[6] Tao F, Zhang L, Lu K, Zhao D (2012) Research on Manufacturing Grid Resource Service Optimal-Selection and Composition Framework. *Enterprise Information Systems* 6(2):237–264.
[7] Odgaard PF, Johnson KE (2013) Wind Turbine Fault Detection and Fault Tolerant Control-an Enhanced Benchmark Challenge. *2013 American Control Conference* 4447–4452.
[8] Wahlström J, Eriksson L (2011) Modelling Diesel Engines with a Variable-Geometry Turbocharger and Exhaust Gas Recirculation by Optimization of Model Parameters for Capturing Non-linear System Dynamics. *Proceedings of the Institution of Mechanical Engineers Part D: Journal of Automobile Engineering* 225(7):960–986.
[9] Bankó Z, Abonyi J (2012) Correlation based Dynamic Time Warping of Multivariate Time Series. *Expert Systems with Applications* 39(17):12814–12823.
[10] Goch G, Wolfgang K, Frank H (2012) Precision Engineering for Wind Energy Systems. *CIRP Annals — Manufacturing Technology* 61(2):611–634.
[11] Hyers RW, McGowan JG, Sullivan KL (2006) Condition Monitoring and Prognosis of Utility Scale Wind Turbines. *Energy Materials* 1(3):187–203.
[12] Huang GB, Zhou HM, Ding XJ, Zhang R (2011) Extreme Learning Machine for Regression and Multiclass Classification. *IEEE Transactions on Systems Man and Cybernetics Part B: Cybernetics* 42(2):513–529.